Monoexponential and advanced diffusion-weighted imaging for hepatic fibrosis staging based on high inter-examiner reliability

Lesheng Huang, MM, *Qian Wei*, MM, *Hui Peng*, MD, *Wanchun Zhang*, BD, *Jiahui Tang*, BD, *Tianzhu Liu*, MM.

ABSTRACT

الأهداف: تحديد الفعالية التشخيصية لتقنيات التصوير الموزون للانتشار المتعدد (DWI) لتحديد مراحل التليف الكبدي (HF) في ظل فرضية الموثوقية العالية بين الفاحصين.

المنهجية: اشتملت الدراسة على المشاركين الذين يعانون من HF المؤكدة بالخزعة وتقسيمهم إلى مجموعات HF المبكرة (EHF) ومجموعات HF المتقدمة (AHF)؛ خدم المتطوعون الأصحاء (HVs) كعناصر ضبط. قام اثنان من الفاحصين بتحليل الحركة غير المتماسكة (IVIM) باستخدام نماذج IVIM–DWI وتصوير التفرطح المنتشر (DKI). قمنا باستخدام Intravoxel غير المتماسكة للحركة DWI و DKI ومعلمات تصوير موتر الانتشار مع معاملات الارتباط (ICCs) البالغة 0.6 وأكثر لإنشاء نماذج الانحدار: HVs مقابل EHF وEHF مقابلAHF.

النتائج: قمنا بتسجيل 48 مريضًا من مرضى HV، و59 مريضًا من مرضى EHF، و38 مريضًا من مرضى AHF. المعدل، والاشعاعي، والتفرطح والمحوري. وتباين كسري. المعدل، شعاعي، وانتشارية محورية. وأظهرت α موثوقية ممتازة (ICCs: 0.80–0.98). أظهر التباين الجزئي للتفرطح، f، ومعامل الانتشار الظاهري موثوقية جيدة (ICCs: 0.69–0.92). وأظهرت معاملات الانتشار الحقيقية (0.58–0.67)، والزائفة (–0.27 0.76)، ومعاملات الانتشار الموزعة (0.58–0.67) موثوقية منخفضة. في نموذج HVs مقابل (مقابل) EHF، قدمت α p=0.008و ADC فروقًا إحصائية p=0.011 (المساحة تحت المنحني [AUC] =0.710). في EHF مقابل نموذج AHF، α p= 0.04 ومعامل الانتشار الموزع (p=0.02) اختلافات كبيرة (AUC: 0.758).

الخلاصة: في ظل فرضية الموثوقية العالية بين الفاحصين، قد تساعد معلمات نموذج الأسي الممتد المشتقة من DWI وIVIM على تنظيم مرحلة HF.

Objectives: To determine the diagnostic efficiencies of multiple diffusion-weighted imaging (DWI) techniques for hepatic fibrosis (HF) staging under the premise of high inter-examiner reliability.

Methods: Participants with biopsy-confirmed HF were recruited and divided into the early HF (EHF) and advanced HF (AHF) groups; healthy volunteers (HVs) served as controls. Two examiners analyzed intravoxel incoherent motion (IVIM) using the IVIM-DWI and diffusion kurtosis imaging (DKI) models. Intravoxel incoherent motion-DWI, DKI, and diffusion tensor imaging parameters with intraclass correlation coefficients (ICCs) of ≥0.6 were used to create regression models: HVs vs. EHF and EHF vs. AHF.

Results: We enrolled 48 HVs, 59 EHF patients, and 38 AHF patients. Mean, radial, and axial kurtosis; fractional anisotropy; mean, radial, and axial diffusivity; and α exhibited excellent reliability (ICCs: 0.80-0.98). Fractional anisotropy of kurtosis, f, and apparent diffusion coefficient showed good reliability (ICCs: 0.69-0.92). The real (0.58-0.67), pseudo- (0.27-0.76), and distributed diffusion coefficients (0.58-0.67) showed low reliability. In the HVs versus (vs.) EHF model, α (p=0.008) and ADC (p=0.011) presented statistical differences (area under curve [AUC]: 0.710). In the EHF vs. AHF model, α (p=0.04) and distributed diffusion coefficient (p=0.02) presented significant differences (AUC: 0.758).

Conclusion: Under the premise of high inter-examiner reliability, DWI and IVIM-derived stretched-exponential model parameters may help stage HF.

Keywords: diffusion-weighted imaging, diffusion kurtosis imaging, diffusion tensor imaging, intravoxel incoherent motion, hepatic fibrosis

In patients with chronic hepatic disease, the development of advanced hepatic fibrosis (AHF) and hepatic cirrhosis has been correlated with significantly increased risks of hepatocellular carcinoma and death.[1] Although untreated hepatic fibrosis (HF) can progress to cirrhosis, timely treatment with anti-fibrosis drugs may reverse HF.[1] Therefore, a reliable method of evaluating HF is essential for monitoring the therapeutic response to anti-fibrosis drugs and for detecting HF progression early. Liver biopsy can be used to evaluate HF; however, this procedure is invasive, and the results rely on the accuracy of sampling and examiner skill. Thus, non-invasive methods are urgently required for HF staging.[2]

Diffusion-weighted imaging (DWI) has been applied to noninvasively quantify HF, but is insufficient for differentiating between HF stages.[3-5] In contrast, intravoxel incoherent motion (IVIM) and diffusion kurtosis imaging (DKI) more accurately reflect the variation in non-Gaussian water diffusion on DWI. Intravoxel incoherent motion is calculated using the biexponential model and multiple b-values, and reflects both tissue perfusion and true water-molecule diffusion. Three quantitative parameters can be derived using IVIM: real diffusion coefficient (D), pseudo-diffusion coefficient (D*), and perfusion fraction (f).[6] The stretched-exponential model of IVIM describes variations in the rates of intravoxel water diffusion represented by the parameter α and the distributed effect of water molecule diffusion indicated by the distributed diffusion coefficient (DDC).[7] However, studies on HF staging using IVIM derived-parameters have yielded inconsistent results.[8-19] Diffusion kurtosis imaging can explain the limitation of water diffusion in the complex tissue microstructure and estimate the excess kurtosis of the probability distribution of diffusion displacement.[20] Studies evaluating the value of DKI in HF staging have also reported inconsistent results.[21-26] Furthermore, most of these studies investigated mean diffusivity (MD) and mean kurtosis (MK), and other DKI-derived parameters, including radial diffusivity (RD), axial diffusivity (AD), axial kurtosis (AK), radial kurtosis (RK), and fractional anisotropy of kurtosis (FAK), are scarcely mentioned in the literature on HF staging.[27]

We consider that the above inconsistent results of IVIM and DKI may be related to the low reliability

of the parameters investigated; moreover, few studies have explored the combined application of all three techniques in HF staging. Therefore, this study aimed to determine the diagnostic efficiencies of parameters derived using DWI, IVIM, and DKI in HF staging based on the premise of high inter-examiner reliability.

Methods. The study protocol was approved by the Institutional Review Board and Ethics Committee of Guangdong Provincial Hospital of Chinese Medicine, Zhuhai, China and was carried out according to the principles of the Helsinki Declaration. All participants signed informed consent forms before being enrolled in the study. We consecutively recruited hepatitis B patients with biopsy-confirmed HF and healthy volunteers (HVs; all aged >18 years) from March 2021 to September 2022. Hepatic fibrosis patients were eligible for this study if they satisfied the following criteria: i) a history of hepatitis; ii) absence of severe ascites; and iii) acceptable image quality. Hepatic fibrosis patients who met either of the subsequent criteria were excluded: i) hepatitis patients without HF on biopsy and ii) inability to undergo biopsy examination. Healthy volunteers were eligible for inclusion in this study if they lacked a history of hepatitis or HF caused by other pathological factors. They were excluded from the study if they satisfied any one of the following criteria: i) any other disease potentially affecting the study results; ii) image quality too poor for taking measurements; and iii) unacceptable image quality.

Hepatitis and HF were diagnosed using histological examination of needle or laparoscopic biopsy specimens and the Scheuer scoring system.[28] The biopsy examination was considered the gold standard for HF staging. Hepatitis patients with HF stages 1 and 2 on histology were assigned to the early hepatic fibrosis (EHF) group, while those with HF stages 3 and 4 were allocated to the AHF group. In both groups, liver biopsy was carried out less than one month after the magnetic resonance imaging (MRI) examination.

Magnetic resonance imaging was carried out on a 3.0 T device (Signa Discovery 750w; GE Healthcare, Pittsburgh, MA, USA) with a 16-channel abdominal coil. Axial, 3-dimensional, in-phase and opposed-phase T1-weighted fast-spin-echo pulse sequences and respiratory-triggered, 2-dimensional, fat-suppressed, axial T2-weighted fast-spin-echo pulse sequences were obtained.[5]

Intravoxel incoherent motion-DWI in the axial plane was carried out with the patient in a supine position and breathing freely. The scanning parameters were as follows: average repetition time, 7000 ms;

average echo time, 69 ms; slice thickness, 6 mm; interslice gap, 1 mm; matrix, 96 × 128; field of view, 340 mm × 272 mm; b-values, 0, 25, 50, 75, 100, 150, 200, 300, 400, 500, 600, and 800 s/mm^2; number of excitations = 1 (b=25-200), 2 (b=0 and 300-500), and 3 (b=600 and 800); and total scan time, 25 minutes.

Diffusion kurtosis imaging in the axial plane was carried out with the patient in a supine position and breathing freely. The scanning parameters were as follows: average repetition time, 2900 ms; average echo time, 75 ms; slice thickness, 6 mm; interslice gap, 1 mm; field of view, 340 mm × 272 mm; matrix = 96 × 128; number of slices, 28; b-values, 0, 800, and 1600 s/mm^2 with 30 directions at each b-value; and total scan time, 10 minutes.

Image post-processing, region of interest (ROI) placement, quality assessment, and image analysis were carried out using an AW 4.6 workstation (GE Healthcare).

Quantitative IVIM-DWI parameters were calculated using the mono-, bi-, and stretched-exponential models. Apparent diffusion coefficient (ADC) was calculated using the monoexponential linear fitting technique and the following equation: $\frac{S(b)}{S_0} = \exp(-b \times ADC)$,

where S(b) represents the mean signal intensity at a given b value, and S0 indicates the mean signal intensity at b=0 s/mm^2.

The biexponential model of IVIM was represented by the following equation:

$$\frac{S(b)}{S_0} = [(1-f) \times \exp(-b \times D)] + [f \times \exp(-b \times D^*)].$$

D was calculated using b values of >200 s/mm^2, and D* was calculated using b values of <200 s/mm^2.

The stretched-exponential model was represented by the following equation: $\frac{S(b)}{S_0} = \exp[-(b \times DDC)]^\alpha$.

The α value varies between 0-1, and higher α values reflect decreased heterogeneity of intravoxel diffusion.

Diffusion kurtosis imaging parameters were derived using the following equation:[27]

$$\frac{S_b}{S_0} = \exp\left(-b \times D + \frac{1}{6}b^2 \times D^2 \times K\right).$$

K describes the degree to which molecular motion deviates from the perfect Gaussian distribution. When K is equal to 0, the above equation evolves into a conventional monoexponential equation.[29,30] Multiple DKI-derived parametric mappings were obtained for the diffusion tensor imaging (DTI) parameters fractional anisotropy (FA), AD, RD, and mean diffusivity (MD) as well as for the DKI parameters MK, AK, RK, and FAK.[31]

The DWI, IVIM-DWI, and DKI scans were analyzed using the post-processing software provided with the AW4.6 workstation (GE Healthcare). Maps of multiple DKI-derived parameters were obtained. Image quality was assessed by an examiner with 17 years of experience in abdominal MRI-based diagnosis. The images that passed the quality assessment were post-processed and quantitatively analyzed by 2 trained examiners with 10 and 16 years of experience, in abdominal MRI-based diagnosis. The examiners worked independently and were blinded to all other patient data. To obtain relatively objective data regarding the right hepatic lobe, we placed 3 discrete ROIs in each right-lobe segment (Couinaud segments V-VIII) while avoiding liver margins, blood vessels, and artifacts. Region of interest position and size (mean: 100 mm^2; range: 80-120 mm^2) were identical on different parametric maps. Apparent diffusion coefficient, D, D*, f, DDC, α, FA, MD, AD, RD, MK, AK, RK, and FAK values were averaged across 12 ROIs (3 ROIs × 4 hepatic segments), and the mean values were finally used for the analysis.

Statistical analysis. Statistical analyses were carried out using the Statistical Package for the Social Sciences, version 26.0 (IBM Corp., Armonk, NY, USA). Continuous variables were presented as mean ± standard deviation (SD). To evaluate the inter-examiner reliability of the DWI, IVIM-DWI, DKI, and DTI measurements, we calculated intraclass correlation coefficients (ICCs) by using a 2-way random model and absolute agreement. ICCs of 0.0-0.2 indicated poor, 0.21-0.4 indicated fair, 0.41-0.6 indicated moderate, 0.61-0.8 indicated good, and 0.81-1 indicated excellent inter-examiner reliability. Multivariate logistic regression models constructed using the enter method were used to analyze parameters that were significantly associated with diagnostic efficiency and had ICCs exceeding 0.60. Between-group differences were compared using the Mann-Whitney U test. Highly correlated independent variables were eliminated using the multicollinearity test. The selected parameters were entered as independent variables, and the different study groups were entered as dependent variables. Receiver operating characteristic (ROC) curves were plotted to determine the diagnostic efficacy of the models. Differences were considered to be statistically significant at *p*-values of <0.05.

Results. We initially recruited 62 EHF patients, 44 AHF patients, and 54 HVs, of whom, 3 EHF patients, 6 AHF patients, and 6 HVs were excluded owing to inadequate image quality. Thus, the study ultimately included 38 AHF (17 women, 21 men) patients, 59 EHF (26 women, 33 men) patients, and 48

HVs (28 women, 20 men). The mean ages of the patients in the AHF group was 43.7 years (range: 27-72 years), 40.4 years (range: 21-62 years) in the EHF group, and 39.2 years (range: 21-69 years) in the HV group. No significant differences were found among the 3 groups in terms of age (AHF versus [vs.] EHF, p=0.11; AHF vs. HVs, p=0.13; EHF vs. HVs, p=0.10) and gender (AHF vs. EHF, p=0.07; AHF vs. HVs, p=0.10; EHF vs. HVs, p=0.09). Representative liver biopsy specimens are shown in Figure 1, and the demographic characteristics of the participants are presented in Table 1.

The inter-examiner reliability was excellent for the DKI parameters MK (ICC: 0.91-0.98), AK (ICC: 0.86-0.96), and RK (ICC: 0.88-0.95); for the DTI parameters FA (ICC: 0.83-0.91), MD (ICC: 0.80-0.96), AD (ICC: 0.80-0.97), and RD (ICC: 0.86-0.96); and for the IVIM-DWI parameter α (ICC: 0.81-0.84). The inter-examiner reliability was good for the DKI-derived FAK (ICC: 0.75-0.92), IVIM-DWI-derived f (ICC: 0.71-0.79), and DWI-derived ADC (ICC: 0.69-0.83). Moderate-to-poor inter-examiner reliability was observed for the DWI-IVIM parameters D (ICC: 0.58-0.67), D* (ICC: 0.27-0.76), and DDC (ICC: 0.58-0.67). The above results are shown in Table 2.

Using the Mann-Whitney U test, we evaluated whether DWI, IVIM, DKI, and DTI parameters with ICCs exceeding 0.60 significantly differed between the different study groups (Table 3). After the test of parallel
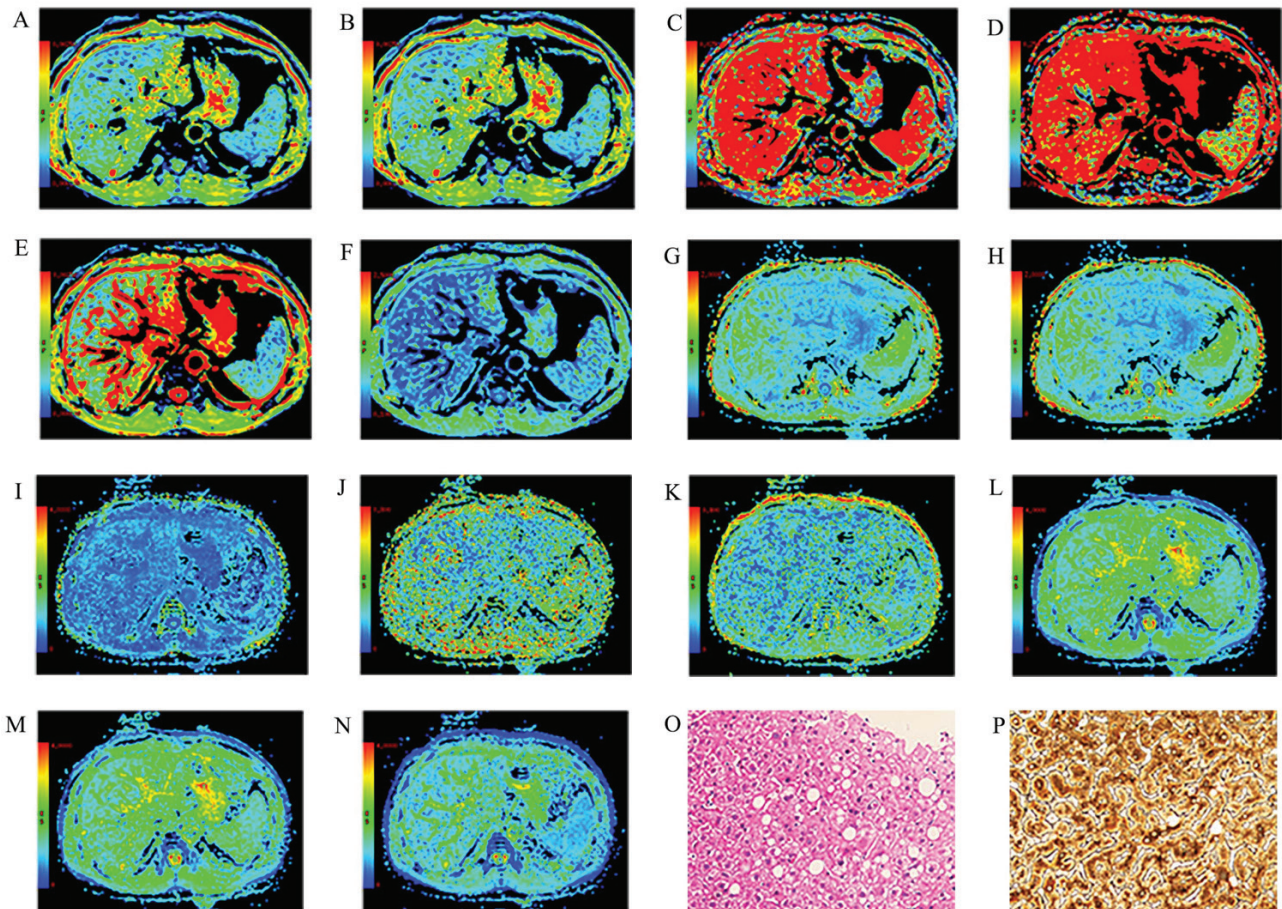
Figure 1 - Illustrations of diffusion-weighted imaging, intravoxel incoherent motion, and diffusion kurtosis imaging parameters, hematoxylin and eosin, and reticular fiber staining. Example of **A)** apparent diffusion coefficient; **B)** real diffusion coefficient; **C)** pseudo-diffusion coefficient; **D)** perfusion fraction; **E)** distributed diffusion coefficient; **F)** water-diffusion heterogeneity within voxels; **G)** fractional anisotropy; **H)** mean diffusivity; **I)** axial diffusivity; **J)** radial diffusivity; **K)** mean kurtosis; **L)** axial kurtosis; **M)** radial kurtosis; and **N)** fractional anisotropy of kurtosis maps in a 58-year-old man from the early hepatic fibrosis group with mild fibrosis (stage 1) and hepatitis (grade 1). **O)** Hematoxylin and eosin staining shows focal necrosis and inflammation around the portal areas, and **P)** reticular fiber staining shows expansion of the portal areas and short fibrous septa.

Table 1 - Demographic and clinical data of the study participants.

Characteristic	HVs	EHF (stages 1 and 2)	AHF (stages 3 and 4)
Number of participants	48 (33.1)	59 (40.7)	38 (26.2)
Age (years), mean±SD (range)†	39.20±13.03 (21-69)	40.40±8.00 (21-62)	43.7±10.20 (27-72)
Gender‡			
Male	20 (13.8)	33 (22.8)	21 (14.5)
Female	28 (19.3)	26 (17.9)	17 (11.7)
Hepatitis grade			
1	N/A	9 (6.2)	0 (0.0)
2	N/A	40 (27.6)	10 (6.9)
3	N/A	10 (6.9)	22 (15.1) Unknown=6
4	N/A	0 (0.0)	0 (0.0)
Hepatic fibrosis stage			
1	N/A	25 (17.2)	0 (0.0)
2	N/A	34 (23.5)	0 (0.0)
3	N/A	0 (0.0)	15 (10.3)
4	N/A	0 (0.0)	23 (15.9)

Values are presented as numbers and percentages (%), please provide the percentages. †There were no significant differences among the groups (*p*>0.05). ‡There was a significant difference between the HVs and AHF group (*p*<0.001). HVs: healthy volunteers, EHF: early hepatic fibrosis, AHF: advanced hepatic fibrosis, SD: standard deviation

Table 2 - Inter-examiner reliability of diffusion-weighted imaging, intravoxel incoherent motion, diffusion kurtosis imaging, and diffusion tensor imaging parameters.

Parameters	HVs	EHF	AHF
		ICC (95% CI)	
Diffusion-weighted imaging			
Apparent diffusion coefficient	0.69 (0.58-0.76)	0.73 (0.77-0.88)	0.83 (0.77-0.88)
Intravoxel incoherent motion			
Real diffusion coefficient	0.58 (0.43-0.78)*	0.67 (0.57-0.75)	0.60 (0.45-0.70)
Pseudo-diffusion coefficient	0.76 (0.68-0.82)	0.51 (0.36-0.62)*	0.27 (0.10-0.47)*
Perfusion fraction	0.71 (0.61-0.78)	0.79 (0.73-0.84)	0.76 (0.67-0.83)
Distributed diffusion coefficient	0.58 (0.44-0.68)*	0.63 (0.52-0.72)	0.67 (0.58-0.74)
Water-diffusion heterogeneity within voxels	0.81 (0.75-0.86)	0.83 (0.78–0.87)	0.84 (0.78-0.88)
Diffusion kurtosis imaging			
Mean kurtosis	0.91 (0.82-0.95)	0.91 (0.85-0.95)	0.98 (0.95-0.99)
Axial kurtosis	0.92 (0.84-0.96)	0.86 (0.75-0.92)	0.96 (0.92-0.98)
Radial kurtosis	0.93 (0.86-0.96)	0.88 (0.79-0.93)	0.95 (0.89-0.97)
Fractional anisotropy of kurtosis	0.92 (0.83-0.96)	0.76 (0.58-0.86)	0.75 (0.50-0.87)
Diffusion tensor imaging			
Fractional anisotropy	0.86 (0.73-0.93)	0.83 (0.71-0.90)	0.91 (0.82-0.95)
Mean diffusivity	0.88 (0.77-0.94)	0.80 (0.65-0.88)	0.96 (0.92-0.98)
Axial diffusivity	0.93 (0.86-0.97)	0.80 (0.65-0.88)	0.97 (0.93-0.98)
Radial diffusivity	0.94 (0.87-0.97)	0.86 (0.76-0.92)	0.96 (0.91-0.98)

*ICC value of <0.6. HVs: healthy volunteers, EHF: early hepatic fibrosis, AHF: advanced hepatic fibrosis, ICC: intraclass correlation coefficient, CI: confidence interval

lines, 2 multivariate regression models were established for differential diagnosis: HVs vs. EHF and EHF vs. AHF.

Based on the screening results, ADC (*p*=0.01), α (*p*=0.01), and FAK (*p*=0.04) formed the HVs vs. EHF regression model, and DDC (*p*=0.02) and α (*p*=0.04) made up the EHF vs. AHF regression model.

In the HVs vs. EHF regression model, ADC (*p*=0.038) and α (*p*=0.015) showed significant differences, while FAK did not (*p*=0.07; AUC: 0.710). To avoid missing potentially significant parameters, we added the FAK parameter to this model and repeated the statistical analysis, but the AUC (0.704) did not improve.

In the EHF vs. AHF regression model, the DDC (*p*=0.001) and α (*p*=0.001) values exhibited significant

Table 3 - Between-group comparison of diffusion-weighted imaging, intravoxel incoherent motion, diffusion kurtosis imaging, and diffusion tensor imaging parameters with high inter-examiner reliability.

Parameters	HVs	EHF	AHF	*P*-values (HVs vs. EHF)	*P*-values (EHF vs. AHF)
Diffusion-weighted imaging					
ADC (10⁻³ mm²/s)	1.80±0.36	1.63±0.35	1.61±0.34	0.01*	0.61
Intravoxel incoherent motion					
D (10⁻³ mm²/s)	1.00±0.28†	0.94±0.25	0.91±0.25	0.31	0.96
D* (10⁻³ mm²/s)	92.65±70.95	114.89±67.76†	83.62±40.62†	0.02*	0.04*
f (%)	31.86±104.71	31.34±86.99	32.11±111.36	0.74	0.88
DDC (10⁻³ mm²/s)	2.91±2.78†	1.98±1.36	3.21±2.51	0.30	0.02*
α (10⁻³ mm²/s)	46.69±11.37	43.20±10.48	48.14±12.07	0.01*	0.04*
Diffusion kurtosis imaging					
MK (10⁻³ mm²/s)	0.77±0.11	0.78±0.12	0.79±0.20	0.48	0.56
AK (10⁻³ mm²/s)	0.74±0.12	0.75±0.14	0.76±0.18	0.69	0.92
RK (10⁻³ mm²/s)	0.74±0.13	0.74±0.15	0.77±0.21	0.57	0.97
FAK (10⁻³ mm²/s)	0.23±0.08	0.28±0.12	0.25±0.08	0.04*	0.30
Diffusion tensor imaging					
FA (10⁻³ mm²/s)	0.23±0.05	0.24±0.07	0.24±0.08	0.35	0.39
MD (10⁻³ mm²/s)	2.01±0.39	1.91±0.40	1.96±0.39	0.37	0.51
AD (10⁻³ mm²/s)	1.39±0.23	1.37±0.25	1.36±0.23	0.74	0.93
RD (10⁻³ mm²/s)	1.11±0.19	1.08±0.17	1.10±0.20	0.43	0.54

Values are presented as mean ± standard deviation (SD). *P-value of <0.05. †intraclass correlation coefficient of <0.6. HVs: healthy volunteers, EHF: early hepatic fibrosis, AHF: advanced hepatic fibrosis, ADC: apparent diffusion coefficient, D: real diffusion coefficient, D*: pseudo-diffusion coefficient, f: perfusion fraction, DDC: distributed diffusion coefficient, α: water-diffusion heterogeneity within voxels, MK: mean kurtosis, AK: axial kurtosis, RK: radial kurtosis, FAK: fractional anisotropy of kurtosis, FA: fractional anisotropy, MD: mean diffusivity, AD: axial diffusivity, RD: radial diffusivity
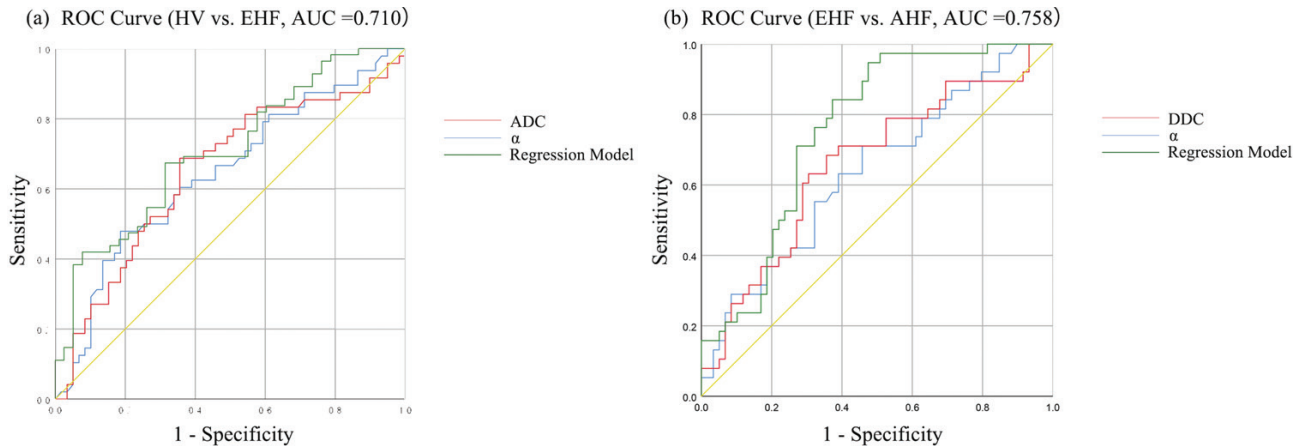
Figure 2 - Statistical results of receiver operating characteristic curve analysis. **A)** Receiver operating characteristic curve analysis of the healthy volunteers vs. early hepatic fibrosis (EHF) model. **B)** Receiver operating characteristic curves of the EHF vs. advanced hepatic fibrosis model. ROC: receiver operating characteristic, HVs: healthy volunteers, EHF: early hepatic fibrosis, AHF: advanced hepatic fibrosis

differences. The AUC for this model was 0.758. The results of the 2 regression models are shown in **Appendix 1** and their ROC curves are shown in **Figure 2**.

Discussion. Our findings showed that D, D*, and DDC were associated with moderate-to-poor inter-examiner reliability (ICC of <0.60) in some groups. However, all DKI- and DTI-derived parameters were excluded because they showed no statistical differences. Finally, only ADC and α were entered into the HVs vs. EHF regression model, and DDC and α were entered into the EHF vs. AHF regression model. Both models presented medium diagnostic efficiency (AUC: 0.710-0.758).

Several studies have hypothesized that ADC values would decrease with the progression of HF, possibly due to the increased connective tissue limiting the Brownian motion of water molecules.[5,32,34,35] However, a high degree of overlap in ADC values was found between different HF stages.[18] Intravoxel incoherent motion and

DKI, which are both derived from DWI technology, have been applied for HF staging in many studies but the conclusions were inconsistent.[18,19,36-38] Considering the above results, we hypothesized that more stable and prominent models could be established by combining DWI-, IVIM-, DKI-, and DTI-derived parameters.

We found that the inter-examiner reliability of D, DDC, and especially D* was low in all groups, which is partially consistent with previous studies.[12,14,15,39] Although several research studies have claimed that D, D*, and DDC have eminent diagnostic efficiency, we had to exclude these parameters to ensure the reliability and stability of the diagnostic models.[14,15,40] Diffusion-weighted imaging, DKI, and DTI parameters showed good-to-excellent reliability, but most DKI and DTI parameters did not significantly differ between the study groups. From previous studies, we consider that there are 2 reasons for this finding: First, the sensitivity and specificity of DKI and DTI in the differentiation of HF stages are poor. Yoon et al[18] and Yang et al[24] concluded that the kurtosis model offered no additional value over the mono- and biexponential models. Second, we only applied 3 b values (0, 800, and 1600 s/mm^2) for DKI, which may have decreased its sensitivity and specificity for HF diagnosis. The unsatisfactory inter-examiner reliability of D* may be related to the high sensitivity of DWI to the perfusion of body fluids; however, D* has shown significant diagnostic efficiency in some studies.[9,10,14] Increasing the reliability of this parameter is an obstinate problem. Although we collected ROIs from multiple right-lobe segments, the reliability of D* remained unsatisfactory. Other novel data-acquisition methods should be attempted to potentially improve the reliability of D*.[35]

The AUC of the ROC curve indicated acceptable diagnostic efficiency of the models in this study, which is consistent with previous results.[12] However, the specificity and sensitivity of the HVs vs. EHF and the specificity and sensitivity of the EHF vs. AHF models, were poor, indicating that the models are not suitable for clinical application. Parameters derived via the stretched-exponential model (DDC and especially α) showed the highest diagnostic efficiency in this study, which suggests that stretched-exponential model parameters may be the most valuable factors for HF staging with good inter-examiner reliability as the premise.[15,38]

Study limitations. First, sample sizes across groups were not even. Second, DKI was possibly carried out with too few b values. Third, histological data could not be obtained from the HVs, potentially decreasing the credibility of the data from these participants. Lastly,

the AUCs of the ROC curves were not as good as those reported in other similar study.[18] We believe that this may be related to the removal of partially derived parameters.

In conclusion, on the premise of high inter-examiner reliability, parameters derived from DWI and the stretched-exponential model of IVIM may be more useful than DKI- and DTI-derived parameters to establish a model for HF staging.

References

1. Ginès P, Krag A, Abraldes JG, Solà E, Fabrellas N, Kamath PS. Liver cirrhosis. *Lancet* 2021; 398: 1359-1376.
2. De Robertis R, D'Onofrio M, Demozzi E, Crosara S, Canestrini S, Pozzi Mucelli R. Noninvasive diagnosis of cirrhosis: a review of different imaging modalities. *World J Gastroenterol* 2014; 20: 7231-7241.
3. Taouli B, Tolia AJ, Losada M, Babb JS, Chan ES, Bannan MA, et al. Diffusion-weighted MRI for quantification of liver fibrosis: preliminary experience. *AJR Am J Roentgenol* 2007; 189: 799-806.
4. Koinuma M, Ohashi I, Hanafusa K, Shibuya H. Apparent diffusion coefficient measurements with diffusion-weighted magnetic resonance imaging for evaluation of hepatic fibrosis. *J Magn Reson Imaging* 2005; 22: 80-85.
5. Bakan AA, Inci E, Bakan S, Gokturk S, Cimilli T. Utility of diffusion-weighted imaging in the evaluation of liver fibrosis. *Eur Radiol* 2012; 22: 682-687.
6. Tao YY, Zhou Y, Wang R, Gong XQ, Zheng J, Yang C, et al. Progress of intravoxel incoherent motion diffusion-weighted imaging in liver diseases. *World J Clin Cases* 2020; 8: 3164-3176.
7. Park JH, Seo N, Chung YE, Kim SU, Park YN, Choi JY, et al. Noninvasive evaluation of liver fibrosis: comparison of the stretched exponential diffusion-weighted model to other diffusion-weighted MRI models and transient elastography. *Eur Radiol* 2021; 31: 4813-4823.
8. Chen C, Wang B, Shi D, Fu F, Zhang J, Wen Z, et al. Initial study of biexponential model of intravoxel incoherent motion magnetic resonance imaging in evaluation of the liver fibrosis. *Chin Med J (Engl)* 2014; 127: 3082-3087.
9. Yoon JH, Lee JM, Baek JH, Shin CI, Kiefer B, Han JK, et al. Evaluation of hepatic fibrosis using intravoxel incoherent motion in diffusion-weighted liver MRI. *J Comput Assist Tomogr* 2014; 38: 110-116.
10. Chung SR, Lee SS, Kim N, Yu ES, Kim E, Kühn B, et al. Intravoxel incoherent motion MRI for liver fibrosis assessment: a pilot study. *Acta Radiol* 2015; 56: 1428-1436.
11. Parente DB, Paiva FF, Oliveira Neto JA, Machado-Silva L, Figueiredo FA, Lanzoni V, et al. Intravoxel incoherent motion diffusion weighted MR imaging at 3.0 T: assessment of steatohepatitis and fibrosis compared with liver biopsy in type 2 diabetic patients. *PLoS One* 2015; 10: e0125653.

12. França M, Martí-Bonmatí L, Alberich-Bayarri Á, Oliveira P, Guimaraes S, Oliveira J, et al. Evaluation of fibrosis and inflammation in diffuse liver diseases using intravoxel incoherent motion diffusion-weighted MR imaging. *Abdom Radiol (NY)* 2017; 42: 468-477.

13. Liang J, Song X, Xiao Z, Chen H, Shi C, Luo L. Using IVIM-MRI and R2* mapping to differentiate early stage liver fibrosis in a rat model of radiation-induced liver fibrosis. *Biomed Res Int* 2018; 2018: 4673814.

14. Sandrasegaran K, Territo P, Elkady RM, Lin Y, Gasparis P, Borthakur G, et al. Does intravoxel incoherent motion reliably stage hepatic fibrosis, steatosis, and inflammation? *Abdom Radiol (NY)* 2018; 43: 600-606.

15. Seo N, Chung YE, Park YN, Kim E, Hwang J, Kim MJ. Liver fibrosis: stretched exponential model outperforms mono-exponential and bi-exponential models of diffusion-weighted MRI. *Eur Radiol* 2018; 28: 2812-2822.

16. Shin HJ, Yoon H, Kim MJ, Han SJ, Koh H, Kim S, et al. Liver intravoxel incoherent motion diffusion-weighted imaging for the assessment of hepatic steatosis and fibrosis in children. *World J Gastroenterol* 2018; 24: 3013-3020.

17. Li T, Che-Nordin N, Wáng YXJ, Rong PF, Qiu SW, Zhang SW, et al. Intravoxel incoherent motion derived liver perfusion/diffusion readouts can be reliable biomarker for the detection of viral hepatitis B induced liver fibrosis. *Quant Imaging Med Surg* 2019; 9: 371-385.

18. Yoon JH, Lee JM, Lee KB, Kim D, Kabasawa H, Han JK. Comparison of monoexponential, intravoxel incoherent motion diffusion-weighted imaging and diffusion kurtosis imaging for assessment of hepatic fibrosis. *Acta Radiol* 2019; 60: 1593-1601.

19. Zawada E, Serafin Z, Dybowska D, Halota W, Wypych A, Nadolska K, et al. Monoexponential and biexponential fitting of diffusional magnetic resonance imaging signal analysis for prediction of liver fibrosis severity. *J Comput Assist Tomogr* 2019; 43: 857-862.

20. Ni P, Lin Y, Zhong Q, Chen Z, Sandrasegaran K, Lin C. Technical advancements and protocol optimization of diffusion-weighted imaging (DWI) in liver. *Abdom Radiol (NY)* 2016; 41: 189-202.

21. Sheng RF, Wang HQ, Yang L, Jin KP, Xie YH, Chen CZ, et al. Diffusion kurtosis imaging and diffusion-weighted imaging in assessment of liver fibrosis stage and necroinflammatory activity. *Abdom Radiol (NY)* 2017; 42: 1176-1182.

22. Sheng RF, Wang HQ, Jin KP, Yang L, Liu H, Ji Y, et al. Histogram analyses of diffusion kurtosis indices and apparent diffusion coefficient in assessing liver regeneration after ALPPS and a comparative study with portal vein ligation. *J Magn Reson Imaging* 2018; 47: 729-736.

23. Sheng RF, Yang L, Jin KP, Wang HQ, Liu H, Ji Y, et al. Assessment of liver regeneration after associating liver partition and portal vein ligation for staged hepatectomy: a comparative study with portal vein ligation. *HPB (Oxford)* 2018; 20: 305-312.

24. Yang L, Rao S, Wang W, Chen C, Ding Y, Yang C, et al. Staging liver fibrosis with DWI: is there an added value for diffusion kurtosis imaging? *Eur Radiol* 2018; 28: 3041-3049.

25. Jia Y, Cai H, Wang M, Luo Y, Xu L, Dong Z, et al. Diffusion kurtosis MR imaging versus conventional diffusion-weighted imaging for distinguishing hepatocellular carcinoma from benign hepatic nodules. *Contrast Media Mol Imaging* 2019; 2019: 2030147.

26. Liu T, Hu J, Liu Y, Chen H, Guo D. Magnetic resonance quantification of non-Gaussian water diffusion in hepatic fibrosis staging: a pilot study of diffusion kurtosis imaging to identify reversible hepatic fibrosis. *Ann Transl Med* 2021; 9: 1569.

27. Wang J, Dou W, Shi H, He X, Wang H, Ge Y, et al. Diffusion kurtosis imaging in liver: a preliminary reproducibility study in healthy volunteers. *MAGMA* 2020; 33: 877-883.

28. Ishak K, Baptista A, Bianchi L, Callea F, De Groote J, Gudat F, et al. Histological grading and staging of chronic hepatitis. *J Hepatol* 1995; 22: 696-699.

29. Verma V, Simone CB 2nd, Krishnan S, Lin SH, Yang J, Hahn SM. The rise of radiomics and implications for oncologic management. *J Natl Cancer Inst* 2017; 109.

30. Lambin P, Leijenaar RTH, Deist TM, Peerlings J, de Jong EEC, van Timmeren J, et al. Radiomics: the bridge between medical imaging and personalized medicine. *Nat Rev Clin Oncol* 2017; 14: 749-762.

31. Hansen B, Jespersen SN. Kurtosis fractional anisotropy, its contrast and estimation by proxy. *Sci Rep* 2016; 6: 23999.

32. Sandrasegaran K, Akisik FM, Lin C, Tahir B, Rajan J, Saxena R, et al. Value of diffusion-weighted MRI for assessing liver fibrosis and cirrhosis. *AJR Am J Roentgenol* 2009; 193: 1556-1560.

33. Girometti R, Furlan A, Bazzocchi M, Soldano F, Isola M, Toniutto P, et al. Diffusion-weighted MRI in evaluating liver fibrosis: a feasibility study in cirrhotic patients. *Radiol Med* 2007; 112: 394-408.

34. Lewin M, Poujol-Robert A, Boëlle PY, Wendum D, Lasnier E, Viallon M, et al. Diffusion-weighted magnetic resonance imaging for the assessment of fibrosis in chronic hepatitis C. *Hepatology* 2007; 46: 658-665.

35. Li YT, Cercueil JP, Yuan J, Chen W, Loffroy R, Wáng YX. Liver intravoxel incoherent motion (IVIM) magnetic resonance imaging: a comprehensive review of published data on normal values and applications for fibrosis and tumor evaluation. *Quant Imaging Med Surg* 2017; 7: 59-78.

36. Fu F, Li X, Chen C, Bai Y, Liu Q, Shi D, et al. Non-invasive assessment of hepatic fibrosis: comparison of MR elastography to transient elastography and intravoxel incoherent motion diffusion-weighted MRI. *Abdom Radiol (NY)* 2020; 45: 73-82.

37. Tosun M, Onal T, Uslu H, Alparslan B, Çetin Akhan S. Intravoxel incoherent motion imaging for diagnosing and staging the liver fibrosis and inflammation. *Abdom Radiol (NY)* 2020; 45: 15-23.

38. Ren H, Liu Y, Lu J, An W, Wang W, Yan T, et al. Evaluating the clinical value of MRI multi-model diffusion-weighted imaging on liver fibrosis in chronic hepatitis B patients. *Abdom Radiol (NY)* 2021; 46: 1552-1561.

39. Lecler A, Savatovsky J, Balvay D, Zmuda M, Sadik JC, Galatoire O, et al. Repeatability of apparent diffusion coefficient and intravoxel incoherent motion parameters at 3.0 Tesla in orbital lesions. *Eur Radiol* 2017; 27: 5094-5103.

40. Hu F, Yang R, Huang Z, Wang M, Zhang H, Yan X, et al. Liver fibrosis: in vivo evaluation using intravoxel incoherent motion-derived histogram metrics with histopathologic findings at 3.0 T. *Abdom Radiol (NY)* 2017; 42: 2855-2863.